Journal of Organometallic Chemistry 897 (2019) 57–63

Contents lists available at ScienceDirect

Journal of Organometallic Chemistry

journal homepage: www.elsevier.com/locate/jorganchem

Heavy alkaline earth π-complexes with doubly-reduced polycyclic aromatic hydrocarbons of variable sizes

Andrew Uresk [a], Natalie J. O'Neil [a, b], Zheng Zhou [a], Zheng Wei [a], Marina A. Petrukhina [a, *]

[a] Department of Chemistry, University at Albany, State University of New York, Albany, NY, 12222, United States
[b] Department of Chemistry and Biochemistry, Utica College, Utica, NY, 13502, United States

ARTICLE INFO

Article history:
Received 12 February 2019
Received in revised form
11 June 2019
Accepted 12 June 2019
Available online 21 June 2019

Keywords:
π-complexation
Heavy alkaline earth metals
Chemical reduction
Mixed ligand complexes
Polycyclic aromatic hydrocarbons
X-ray diffraction •

ABSTRACT

Barium (II) π-complexes with two planar polycyclic aromatic hydrocarbons (PAHs), anthracene and fluoranthene, have been prepared by direct alkaline earth metal reduction reactions in THF in the presence of 1,2-diiodoethane (DIE), used as an activator. The products have been crystallographically characterized to reveal their mixed-ligand composition, $\{[Ba(I)(THF)_3]_2^{2+}[C_{14}H_{10}]^{2-}\}$ (**1**) and $\{[Ba(I)(THF)_3]_2^{2+}[C_{16}H_{10}]^{2-}\}$ (**2**). A similar strontium (II) product, $\{[Sr(I)(THF)_4]_2^{2+}[C_{10}H_8]^{2-}\}$ (**3**), has been synthesized using potassium-naphthalenide ligand-exchange reaction starting with SrI_2. In **1** and **2**, Ba(II) ions are π-complexed by doubly-reduced PAHs with the planarity of the dianions being preserved upon reduction and metal binding. In contrast, the naphthalene dianion in **3** adopts a non-planar geometry with a dihedral angle of 15.2°. The $M-C_{centroid}$ distances of 2.754 (6) Å and 2.755 (14) Å in **1** and **2**, respectively, are longer than that in **3** (2.600 (2) Å). The coordination environment of alkaline earth metal ions is completed by iodide ligands and coordinated THF molecules. The X-ray structural investigation confirmed the formation of the iodide-bridged 1D polymers in barium products, $\{[Ba(\mu\text{-}I)(THF)_3]_2^{2+}[C_{14}H_{10}]^{2-}\}_\infty$ (**1**) and $\{[Ba(\mu\text{-}I)(THF)_3]_2^{2+}[C_{16}H_{10}]^{2-}\}_\infty$ (**2**) *vs.* a discrete strontium complex with terminal iodide ligands in **3**.

1. Introduction

Organometallic chemistry of Group 2 metals has been expanding over the years [1,2]. However, the developments of late Group 2 metals are still lagging behind the progress achieved with early alkaline earth metals. For two heavy congeners of Group 2, strontium and barium, the organometallic chemistry is largely centered around cyclopentadiene (CP) and cyclooctatetraene (COT) ligands [3,4] with a very limited number of other π-systems engaged in complexation. Although the studies on reduction of planar polycyclic aromatic hydrocarbons (PAHs) with the alkaline earth metals go back to 1905 [5], only a handful of strontium and barium complexes with selected PAHs (Scheme 1) such as fluorene [6] and its hypersilyl-fluorene (hSi-Flu) derivative [7], indene and diisopropyl indene [8], as well as dibenzopentalene [9] have been crystallographically characterized to date. Besides fundamental interest in this chemistry, the resulting products are used in synthetic organic [10,11] and polymer chemistry [12], and materials synthesis [3c]. The superconductivity of fullerenes doped with Group 2 metals has also attracted attention [13]. Moreover, the organometallic compounds of alkaline earth metals have found applications in catalysis, stimulated by their high abundance in the earth's crust [14].

The progress of late Group 2 metal chemistry is plagued with complications stemming from their low reactivity and high insolubility. In contrast to alkali metals, [15] the direct use of alkaline earth metals as reducing agents requires their prior activation. Several methods have been reported in the literature, varying from physical surface activation to chemical activation techniques. The methods utilizing metal vapours [16] and activated metal powders [17], liquid ammonia [18], or the entrainment approach [19] all rely on activation of the elemental form of metals. The entrainment method was successfully applied for the activation of magnesium metal, as first shown by Grignard in 1934 [19a]. Advances to this method developed by Beckler and co-workers in 1959 have increased the yield and made it a viable activation strategy to access Group 2 metal compounds [19b]. This method still serves as an effective activation approach; however, it is mainly limited to magnesium in the literature [20–22]. We have recently shown that this method could also be successful in the activation of calcium

* Corresponding author.
E-mail address: mpetrukhina@albany.edu (M.A. Petrukhina).

https://doi.org/10.1016/j.jorganchem.2019.06.011
0022-328X/

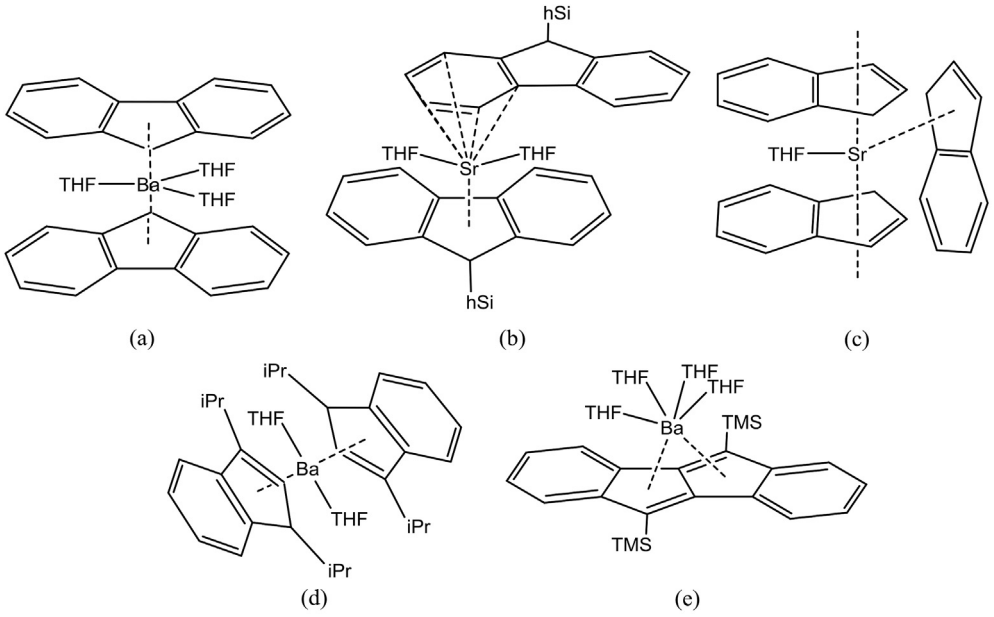

Scheme 1. Models of structurally characterized π-complexes of strontium (II) and barium (II) with planar PAH anions.

metal [23], but no expansion to include heavier Group 2 congeners has been reported.

Additional activation methods such as halide metathesis [24] and transamination [25] utilize synthetic techniques that do not rely on the elemental metals. These chemical methods allow for more precise reaction reproducibility and generally produce products in good yield, although the by-products formed during the reactions can be difficult to remove. Therefore, further development of effective activation methods is still needed in order to reinvigorate and expand the chemistry of the alkaline earth metals.

In this work, we set to investigate the reduction behavior of heavy Group 2 metals using planar polycyclic aromatic hydrocarbons as π-ligands. We selected the chemical activation method known to be successful for early Group 2 metals [22,23] and compared it with the halide metathesis reaction. We report two new barium (II) complexes with $[C_{14}H_{10}]^{2-}$ and $[C_{16}H_{10}]^{2-}$ anions as well as the strontium (II) complex with $[C_{10}H_8]^{2-}$ and provide their structural characterization by single-crystal X-ray diffraction.

2. Results and discussion

To access new π-complexes of heavy Group 2 metals we have chosen an alkyl halide for activation. We opted to use 1,2-diiodoethane (DIE) for the following reasons. DIE is a solid at room temperature and this makes it easy to measure for quantitative use in the subsequent reactions. The byproducts formed, ethane gas and the metal iodide, are innocuous and can be easily removed from the reaction mixture. The additional benefit to this synthetic method is that the solid DIE can be directly added to the reaction mixture in a one-pot synthesis. Overall, the use of one-pot synthetic techniques with a minimized number of steps is favored in preparation of very air-sensitive and reactive products.

With the goal of developing effective activation techniques suitable for barium metal, we selected two planar PAHs, anthracene ($C_{14}H_{10}$) and fluoranthene ($C_{16}H_{10}$), for chemical reduction reactions. The optimal conditions for these reactions rely on the excess of metal (*ca.* 5–7 eq.) in respect to the amount of a PAH ligand. We found that *ca.* 10% of activator is required to facilitate the completion of reduction reactions within 1–3 days. The color of the solution (characteristic of reduction) became more intense in the reactions with 10% of DIE, thus indicating an increase in the reaction rate. It was also expected that the amount of active metal that can react with the ligand should increase with an increase in the amount of DIE in the reaction.

In the course of this study, two new barium products have been isolated in single-crystalline form and both were crystallographically characterized. The barium (II) anthracene complex, **1**, was synthesized using anthracene, barium metal, and DIE in THF at room temperature (see Experimental part for details). Upon layering the THF reaction solution with hexanes at 10 °C, brown block-shaped crystals of good quality were obtained in moderate yield. The X-ray crystallographic study revealed that the product has the $\{[Ba(I)(THF)_3]_2^{2+}[C_{14}H_{10}]^{2-}\}$ composition. The UV–vis spectrum of **1** dissolved in THF shows absorbance in the ultraviolet region between 325 and 386 nm along with peaks centered at 452 nm and 607 nm, which are characteristic of the dianion of anthracene (Fig. S1). The UV–vis spectrum of **1** is in good agreement with that reported for the anthracene dianion with sodium counterions, which exhibits a maximum absorbance at 600 nm [26].

In the crystal structure of **1**, an anthracene dianion has two barium ions bound symmetrically in an η^6-fashion to opposing peripheral six-membered rings (Fig. 1). The Ba–C distances range from 3.041 (6) Å to 3.174 (6) Å with an average distance of 3.096 (6) Å and a Ba–$C_{centroid}$ distance of 2.754 (6) Å. These distances are similar to those found in analogous barium (II) π-complexes [6,8,9]. Each barium has three THF molecules coordinated with the Ba–O_{THF} bond length distances ranging from 2.719 (4) Å to 2.777 (4) Å (Ba–O_{avg}, 2.742 (4) Å).

In the solid-state, **1** crystallizes as an 1D coordination polymer, $\{[Ba(I)\ (THF)_3]_2^{2+}[C_{14}H_{10}]^{2-}\}_\infty$, propagating through the formation of iodide bridges between each pair of barium (II) ions (Fig. 1). Each barium (II) ion is bound to two iodide ligands with the Ba–I bond length distances of 3.4820 (6) Å and 3.5444 (6) Å. The Ba–I–Ba and I–Ba–I bond angles are 97.474 (11)° and 82.525 (11)°, respectively.

In the $[C_{14}H_{10}]^{2-}$ dianion, the C–C bond length distances range from 1.374 (9) Å to 1.453 (8) Å and are within ±0.055 Å from those found in the neutral ligand (Table 1) [27]. Notably, the deviation of each carbon atom from a plane created through the C1–C14 atoms

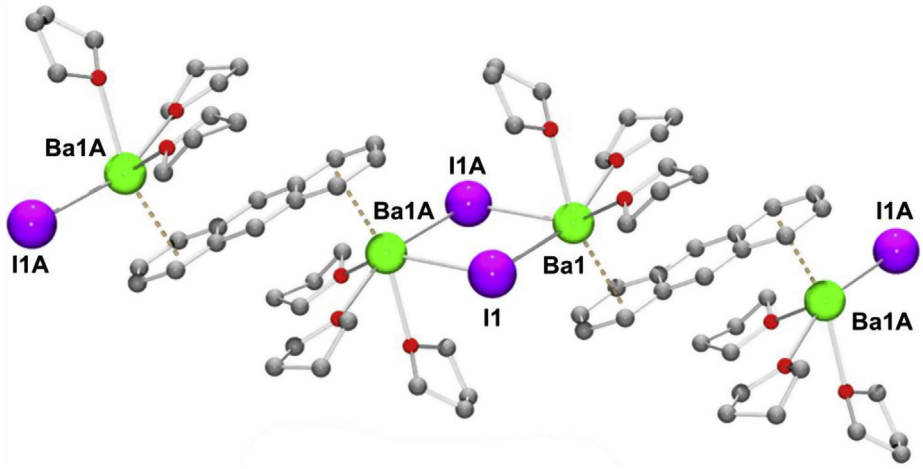

Fig. 1. Fragment of the polymeric structure of $\{[Ba(I)(THF)_3]_2^{2+}[C_{14}H_{10}]^{2-}\}_\infty$ in **1**. Hydrogen atoms are removed for clarity. Barium (green), iodine (purple), carbon (grey), and oxygen (red). (For interpretation of the references to color in this figure legend, the reader is referred to the Web version of this article.)

Table 1
C–C bond length distances (Å) in neutral anthracene [27b] and $[C_{14}H_{10}]^{2-}$ in **1**.

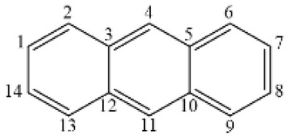

C–C	$C_{14}H_{10}$	$[C_{14}H_{10}]^{2-}$	Δ (Å)	C–C	$C_{14}H_{10}$	$[C_{14}H_{10}]^{2-}$	Δ (Å)
C1–C2	1.359 (2)	1.414 (9)	0.055	C9–C10	1.429 (2)	1.426 (8)	−0.003
C2–C3	1.429 (2)	1.426 (8)	0.003	C10–C11	1.398 (2)	1.410 (9)	0.012
C3–C4	1.398 (2)	1.410 (9)	0.012	C11–C12	1.398 (2)	1.408 (8)	0.010
C4–C5	1.398 (2)	1.408 (9)	0.010	C12–C13	1.432 (2)	1.405 (8)	−0.027
C5–C6	1.432 (2)	1.405 (8)	−0.027	C13–C14	1.363 (2)	1.418 (8)	0.055
C6–C7	1.363 (2)	1.418 (8)	0.055	C1–C14	1.424 (2)	1.374 (9)	−0.050
C7–C8	1.424 (2)	1.374 (9)	−0.050	C3–C12	1.436 (2)	1.453 (8)	0.017
C8–C9	1.359 (2)	1.414 (9)	0.055	C5–C10	1.436 (2)	1.453 (8)	0.017

*Δ is calculated by subtracting the bond length of neutral anthracene from that for $[C_{14}H_{10}]^{2-}$.

of anthracene core is calculated to be within 0.019 Å. Thus, the reduction and binding of the large barium (II) ions do not affect the planarity of the anthracene dianion.

A careful literature search revealed that only a very few anthracene dianions with either the alkali (Li, K) or early alkaline earth (Mg) metals have been structurally characterized to date [28]. The product with lithium counterions exists as a contact-ion pair (CIP), in which the anthracene dianion deviates from planarity by 0.214 Å due to the metal binding to the central ring of the ligand [28a]. Interestingly, despite all the differences between lithium and yttrium, analogous geometrical deformations of $[C_{14}H_{10}]^{2-}$ are observed in the dinuclear π-complex of yttrium [29]. The product with potassium ions exhibits an unusual triple-decker sandwich structure consisting of two anthracene monoanion-radicals and one dianion, all retaining their planarity [28c]. In contrast, the anthracene dianion experiences folding of 28.6° in its complex with magnesium ions bound to the bridgehead C-atoms in a polar covalent fashion [28b]. The reported examples illustrate coordination and structural versatility of the $[C_{14}H_{10}]^{2-}$ ligand upon metal binding. The new complex **1** now adds the first 1D polymeric structure to the family.

The barium fluoranthene complex, **2**, was synthesized using fluoranthene, barium metal, and DIE in THF at room temperature (see Experimental part for details). Upon layering the THF reaction solution with hexanes at 10 °C, brown block-shaped crystals of good quality were deposited in moderate yield. The X-ray crystallographic study revealed that the product has the $\{[Ba(I)(THF)_3]_2^{2+}[C_{16}H_{10}]^{2-}\}$ composition. The UV–vis spectrum of **2** dissolved in THF shows absorbance in the ultraviolet region between 335 and 398 nm and a maximum at 447 nm characteristic of the fluoranthene dianion (Fig. S1). The UV–vis spectrum of **2** is in good agreement with those reported for the fluoranthene dianion isolated with sodium or lithium countercations [30].

In the crystal structure of **2**, a fluoranthene dianion has two crystallographically independent barium ions bound symmetrically in an η^6-fashion to opposing six-membered rings (Fig. 2). All bond distances discussed below are averaged due to a similar environment of Ba (1) and Ba (2) ions. The Ba–C bond length distances range from 2.983 (14) Å to 3.257 (14) Å with an average distance of 3.097 (14) Å and a Ba–$C_{centroid}$ distance of 2.755 (14) Å. These distances are similar to those found in analogous barium (II) π-complexes [6,8]. Each barium has three THF molecules coordinated with the Ba–O_{THF} bond length distances ranging from 2.657 (9) Å to 2.845 (9) Å (Ba–O_{avg}, 2.749 (9) Å).

In the solid state, **2** crystallizes as a coordination polymer, $\{[Ba(I)(THF)_3]_2^{2+}[C_{16}H_{10}]^{2-}\}_\infty$, propagating through the formation of iodide bridges between each pair of barium (II) ions (Fig. 2). Each barium (II) ion is bound to two iodide ligands with Ba–I (1) and

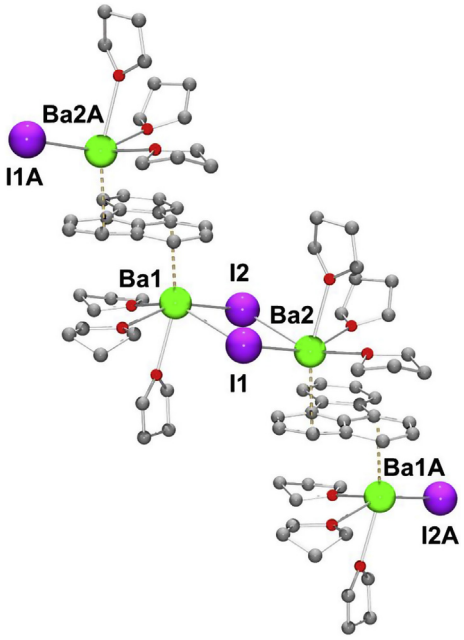

Fig. 2. Fragment of the polymeric structure of $\{[Ba(I)(THF)_3]_2^{2+}[C_{16}H_{10}]^{2-}\}_\infty$, **2**. Hydrogen atoms are removed for clarity. Oxygen (red), carbon (grey). (For interpretation of the references to color in this figure legend, the reader is referred to the Web version of this article.)

Ba–I (2) bond length distances of 3.4683 (11) Å and 3.5070 (12) Å, respectively. The Ba (1)–I (1)–Ba (2) and Ba (1)–I (2)–Ba (2) bond angles are 98.92 (3)° and 97.48 (3)°, while the I (1)–Ba (1)–I (2) and I (1)–Ba (2)–I (2) bond angles are 81.75 (3)° and 81.85 (3)°, respectively. The average Ba–I–Ba and I–Ba–I angles in **2** are very similar to those in **1**.

In the $[C_{16}H_{10}]^{2-}$ dianion, the C–C bond length distances range from 1.320 (20) Å to 1.474 (18) Å and are within ±0.105 Å from neutral fluoranthene (Table 2) [31]. Notably, the deviation of each carbon atom from a plane created through the C1–C16 atoms of fluoranthene core is calculated to be within 0.076 Å. Similar to **1**, the reduction and binding of the barium (II) ions do not affect the planarity of the fluoranthene dianion in **2**.

A careful literature search found that only three examples of fluoranthene dianions have been prepared with the Group 1 metals (Li and Na) [32], making complex **2** to be the first structurally characterized with a Group 2 metal. Similar to **2**, the planarity of the fluoranthene dianion core was preserved in the reported alkali metal products.

The strontium naphthalene complex, **3**, was synthesized using a ligand exchange reaction between potassium naphthalenide and strontium (II) iodide in THF at room temperature (see Experimental part for details). After one week, red-orange block-shaped crystals of good quality were deposited in moderate yield from the reaction mixture. The X-ray crystallographic study revealed that the product has the) ($\{[Sr(I)(THF)_4]_2^{2+}[C_{10}H_8]^{2-}\}$ composition. The UV–vis spectrum of **3** dissolved in THF shows absorbance in the ultraviolet region between 310 and 361 nm along with peaks centered at 449 nm and 573 nm, which are characteristic for the dianion of naphthalene (Fig. S2). For comparison, the naphthalene dianions isolated with lithium [33], europium [34], and lanthanum [34] exhibit strong bands at 550 nm, 575 nm, and 604 nm, respectively.

In the crystal structure of **3**, a naphthalene dianion has two strontium (II) ions bound symmetrically in an η^4-fashion to opposing six-membered rings (Fig. 3). The Sr–C bond length distances range from 2.837 (2) Å to 2.9626 (19) Å with an average distance of 2.890 (2) Å and a Sr–$C_{centroid}$ distance of 2.600 (2) Å. An analysis of binding shows that the strontium (II) ion is shifted towards the outside C5–C6 bond (See numbering scheme in Table 3). The Sr–π contacts in **3** are similar to those found in the analogous bis(indenyl)strontium complex [8]. Each strontium has four THF molecules coordinated with the Sr–O_{THF} bond length distances ranging from 2.5507 (14) Å to 2.6586 (14) Å (Sr–O_{avg}, 2.6044 (15) Å).

Unlike the 1D polymeric barium (II) structures, **3** crystallizes in the solid-state as a discrete complex, $\{[Sr(I)(THF)_4]_2^{2+}[C_{10}H_8]^{2-}\}$ (Fig. 3). Each strontium (II) ion is coordinated to one iodide ligand with a Sr–I bond length distance of 3.3410 (3) Å. This structural difference between **1**–**2** and **3** may be attributed to a large ionic radii of Ba(II) *vs.* that of Sr(II) (1.35 Å *vs.* 1.13 Å) [35].

Upon acquisition of two electrons there is a change in the naphthalene C–C bond pattern (Table 3). In the $[C_{10}H_8]^{2-}$ dianion, the C–C bond length distances range from 1.375 (3) Å to 1.454 (4) Å and are within ±0.063 Å from those found in the neutral

Table 2
C–C bond lengths (Å) in neutral fluoranthene [31] and $[C_{16}H_{10}]^{2-}$ in **2**.

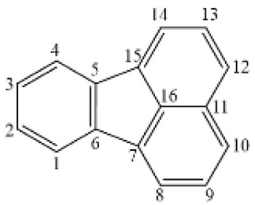

C–C	$C_{16}H_{10}$	$[C_{16}H_{10}]^{2-}$	Δ (Å)	C–C	$C_{16}H_{10}$	$[C_{16}H_{10}]^{2-}$	Δ (Å)
C1–C2	1.395 (3)	1.372 (19)	−0.023	C11–C12	1.426 (3)	1.454 (19)	0.028
C2–C3	1.393 (3)	1.380 (20)	−0.013	C12–C13	1.377 (3)	1.418 (19)	0.041
C3–C4	1.395 (3)	1.350 (20)	−0.045	C13–C14	1.420 (3)	1.320 (20)	−0.100
C4–C5	1.388 (3)	1.394 (18)	0.006	C14–C15	1.370 (3)	1.475 (18)	0.105
C5–C6	1.420 (3)	1.458 (17)	0.038	C15–C16	1.417 (3)	1.436 (17)	0.019
C6–C7	1.481 (3)	1.431 (18)	−0.050	C1–C6	1.387 (3)	1.423 (18)	0.036
C7–C8	1.371 (3)	1.434 (18)	0.063	C5–C15	1.476 (3)	1.405 (18)	−0.071
C8–C9	1.417 (3)	1.410 (20)	−0.007	C7–C16	1.416 (3)	1.398 (18)	−0.018
C9–C10	1.387 (3)	1.428 (18)	0.041	C11–C16	1.394 (3)	1.433 (16)	0.039
C10–C11	1.424 (3)	1.396 (19)	−0.028				

*Δ is calculated by subtracting the bond length of neutral fluoranthene from that for $[C_{16}H_{10}]^{2-}$.

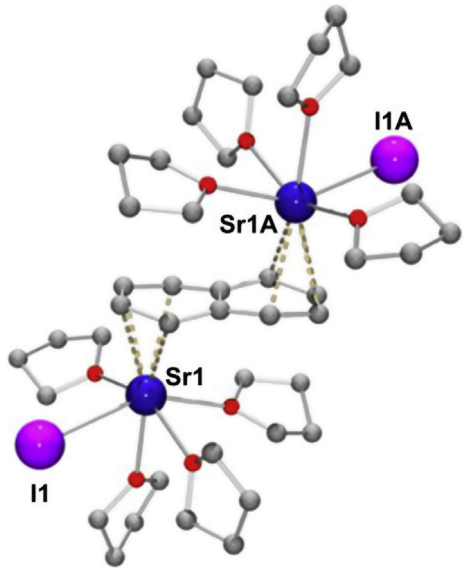

Fig. 3. Molecular structure of $\{[Sr(I)(THF)_4]_2^{2+}[C_{10}H_8]^{2-}\}$, **3**. Hydrogen atoms are removed for clarity. Strontium (blue), iodine (purple), carbon (grey), and oxygen (red). (For interpretation of the references to color in this figure legend, the reader is referred to the Web version of this article.)

ligand [36]. However, the core of the dianion is not planar and adopts a bend geometry with a dihedral angle of 15.2° between the C4–C5–C6–C7 and C7–C8–C3–C4 planes. The nonplanarity of $[C_{10}H_8]^{2-}$ could be responsible for the observed η^4-coordination of Sr(II) in **3** *vs.* η^6-coordination of Ba(II) in **1** and **2**. A literature search has found two structurally characterized examples of naphthalene dianion with lithium counterions [37] and several more with lanthanides [29,38]. The observed core deformation of $[C_{10}H_8]^{2-}$ in the new strontium complex **3** is in agreement with values reported in literature[[29,34,37,38].

3. Experimental part

3.1. Materials and methods

All manipulations were carried out using break-and-seal [39] and glove-box techniques under an atmosphere of argon. Solvents (THF and hexanes) were dried over Na/benzophenone and distilled prior to use. THF-d_8 was dried over NaK alloy and vacuum-transferred. Strontium and barium metals were purchased from Sigma Aldrich. 1,2-Diiodoethane (99%) was purchased from Sigma Aldrich and used as received. Naphthalene, anthracene and fluoranthene were purchased from Sigma Aldrich and doubly sublimed prior to use at 60 °C, 180 °C and 90 °C, respectively. The UV–vis spectra were recorded on a PerkinElmer Lambda 35 spectrometer. The ^{1}H NMR spectra of **1** and **2** were measured on a Bruker Advance III spectrometer at 400 MHz, while the ^{1}H spectra of **3** were recorded on a Bruker Ascend-500 spectrometer at 500 MHz. All spectra were referenced to the residual resonances of THF-d_8 ($\delta = 3.62$ ppm and 1.79 ppm) [40]. The extreme air- and moisture sensitivity of the isolated crystals **1**–**3** prevented the collection of elemental analysis data.

Preparation of $\{[Ba(I)(THF)_3]_2^{2+}[C_{14}H_{10}]^{2-}\}$ (1)

In the glovebox, a glass system was loaded with anthracene (10.0 mg, 0.056 mmol), Ba metal (48 mg, 0.35 mmol), and DIE (12.0 mg, 0.043 mmol). Then anhydrous THF (2.0 mL) was added to the system via syringe. The solution turned yellow immediately and further reduced to a light blue color after stirring at room temperature for 1 h. Over the next 24 h, the solution slowly darkened to a dark blue-purple color. After filtration, the dark blue-purple solution was layered with hexanes (2.0 mL). The glass tube was sealed under vacuum and placed in the fridge at 10 °C. Dark brown block-shaped crystals were observed after 2 weeks. Yield: 20 mg, 32%. UV–vis (THF, nm): $\lambda_{max} = 452$, 607 (Fig. S1). ^{1}H NMR (400 MHz, THF-d_8, 25 °C, ppm): $\delta = 6.87$ (4H), 6.71 (4H), 4.54 (2H), 3.62 (C_4H_8O), 1.77 (C_4H_8O) (Fig. S3).

Preparation of $\{[Ba(I)(THF)_3]_2^{2+}[C_{16}H_{10}]^{2-}\}$ (2)

In the glovebox, a glass apparatus was loaded with fluoranthene (10.0 mg, 0.049 mmol), Ba metal (45 mg, 0.327 mmol), and DIE (10.8 mg, 0.038 mmol). Then anhydrous THF (2.2 mL) was added to the system via syringe. The solution turned yellow immediately and further reduced to a light brown color after stirring at room temperature for 1 h. Over the next 24 h the solution slowly darkened to a dark brown color. After filtration, the dark brown solution was layered with hexanes (2.0 mL). The glass tube was sealed under vacuum and placed in the fridge at 10 °C. Dark brown block-shaped crystals were observed after 2 weeks. Yield: 20 mg, 35%. UV–vis (THF, nm): $\lambda_{max} = 447$ (Fig. S1). ^{1}H NMR (400 MHz, THF-d_8, 25 °C, ppm): $\delta = 6.99$ (2H), 6.38 (2H), 5.04 (2H), 3.42 (2H), 3.29 (2H), 3.62 (C_4H_8O), 1.76 (C_4H_8O) (Fig. S4).

Table 3
C–C bond lengths (Å) in neutral naphthalene [36] and $[C_{10}H_8]^{2-}$ in **3**.

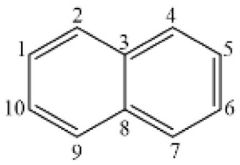

C–C	$C_{10}H_8$	$[C_{10}H_8]^{2-}$	Δ (Å)	C–C	$C_{10}H_8$	$[C_{10}H_8]^{2-}$	Δ (Å)
C1–C2	1.376 (3)	1.437 (3)	0.061	C7–C8	1.424 (3)	1.425 (3)	0.001
C2–C3	1.424 (3)	1.425 (3)	0.001	C8–C9	1.423 (3)	1.424 (3)	0.001
C3–C4	1.423 (3)	1.424 (3)	0.001	C9–C10	1.376 (3)	1.439 (3)	0.063
C4–C5	1.376 (3)	1.439 (3)	0.063	C1–C10	1.414 (3)	1.376 (3)	−0.039
C5–C6	1.414 (3)	1.376 (3)	−0.038	C3–C8	1.424 (3)	1.453 (4)	0.029
C6–C7	1.376 (3)	1.437 (3)	0.061				

*Δ is calculated by subtracting the bond length of neutral naphthalene from that of $[C_{10}H_8]^{2-}$.

Preparation of $\{[Sr(I)(THF)_4]_2^{2+}[C_{10}H_8]^{2-}\}$ (3)

In the glovebox, a flask was loaded with naphthalene (76 mg, 0.593 mmol) and potassium metal (23 mg, 0.593 mmol). Then 1.5 mL THF was added to the mixture and it was sonicated for 2 h resulting in a deep green solution. A separate flask was loaded with strontium iodide (156 mg, 0.457 mmol) in the glovebox followed by the addition of 1.5 mL THF. The mixture was sonicated for 2 h resulting in a fine white power suspended in THF. The potassium-naphthalenide solution was then filtered into the strontium iodide suspension, producing a blue-purple reaction mixture which was stirred for 2 h. The solvent was removed and dark blue-purple solid was washed with fresh THF (1 mL). Then THF (*ca.* 1 mL) was added to the system and the flask was kept in the glovebox at room temperature. Dark red-brown block-shaped crystals were observed after 1 week at the bottom of the storage flask. Yield: 200 mg, 30%. UV–vis (THF, nm): $\lambda_{max} = 449$, 573 (Fig. S2). ^{1}H NMR (500 MHz, THF-d_8, 25 °C, ppm): $\delta = 7.06$ (4H), 5.88 (4H), 3.62 (C_4H_8O), 1.76 (C_4H_8O) (Fig. S5).

3.2. Crystal structure determinations and refinement of **1**, **2**, and **3**

Data collections were performed on a Bruker D8 VENTURE X-ray diffractometer with PHOTON 100 CMOS shutterless mode detector equipped with a Mo-target X-ray tube ($\lambda = 0.71073$ Å) at $T = 100$ (2) K. Data reduction and integration were performed with the Bruker software package SAINT (version 8.38A) [41]. Data were corrected for absorption effects using the empirical methods as implemented in SADABS (version 2016/2) [42]. The structures were solved by SHELXT (version 2018/2) [43] and refined by full-matrix least-squares procedures using the Bruker SHELXTL (version 2018/3) [44] software package. In **1**, **2**, and **3**, all non-hydrogen atoms were refined anisotropically. The H-atoms of **1**, **2** and **3** were included at calculated positions and refined as riders, with $U_{iso}(H) = 1.2\ U_{eq}(C)$. In **1**, the structure was refined as a two-component non-merohedral twin with the BASF value refined to 0.4980. In **2**, each unit cell contained ten *n*-hexane molecules that were found to be severely disordered and removed by the SQUEEZE subroutine in PLATON (version 230418) [45]. The total void volume was 1209 Å^3 indicated by PLATON, which is equivalent to 23.27% of the unit cell's total volume. In **3**, reflections −1 0 1, 0 0 2, 2 0 1, 1 2 3, and 2 0 2 are omitted during refinement since they were truncated by the beam stop. For further crystal and data collection details see Table S1. CCDC 1889856–1889858 contain the supplementary crystallographic data for **1**, **2**, and **3**, respectively. These data can be obtained free of charge from the Cambridge Crystallographic Data Centre via www.ccdc.cam.ac.uk/data_request/cif.

4. Conclusions

In this work, the chemical activation method of barium metal with 1,2-diiodoethane has been tested in the reduction reactions with selected planar PAHs. Two new barium complexes have been isolated and crystallographically characterized to confirm their mixed-ligand composition, namely $\{[Ba(I)(THF)_3]_2^{2+}[C_{14}H_{10}]^{2-}\}_\infty$ and $\{[Ba(I)(THF)_3]_2^{2+}[C_{16}H_{10}]^{2-}\}_\infty$. In both, the planarity of the doubly-reduced PAH ligands is preserved. A similar strontium product, $\{[Sr(I)(THF)_4]_2^{2+}[C_{10}H_8]^{2-}\}$, has been isolated using a different synthetic route based on the ligand exchange reaction. In contrast to above, the deformation from planarity is observed for the naphthalene dianion in the strontium complex, similar to the previously reported cases with alkali and lanthanide counter-cations. The new mixed-ligand π-complexes expand the organometallic chemistry of the late Group 2 metals and show the need for further development of their activation methods.

Acknowledgment

Financial support of this work from the National Science Foundation (CHE-1608628 and MRI-1337594) is gratefully acknowledged.

Appendix A. Supplementary data

Supplementary data to this article can be found online at https://doi.org/10.1016/j.jorganchem.2019.06.011.

References

[1] (a) T.P. Hanusa, Polyhedron 9 (1990) 1345;
(b) T.P. Hanusa, Coord. Chem. Rev. 210 (2000) 329;
(c) C.N. de Bruin-Dickason, G.B. Deacon, C. Jones, P.C. Junk, M. Wiecko, Eur. J. Inorg. Chem. 7 (2019) 1030.
[2] (a) W.D. Buchanan, D.G. Allis, K. Ruhlandt-Senge, Chem. Commun. 46 (2010) 4449;
(b) S. Krieck, H. Görls, M. Westerhausen, J. Am. Chem. Soc. 132 (2010) 12492;
(c) A. Torvisco, K. Ruhlandt-Senge, Top. Organomet. Chem. 45 (2013) 1.
[3] (a) R.A. Williams, T.P. Hanusa, J.C. Huffman, J. Chem. Soc., Chem. Commun. (1988) 1045;
(b) M. Rieckhoff, U. Pieper, D. Stalke, F.T. Edelmann, Angew. Chem. 105 (1993) 1102;
(c) M.J. Harvey, K.T. Quisenberry, T.P. Hanusa, V.G. Young Jr., Eur. J. Inorg. Chem. (2003) 3383;
(d) M.J. Harvey, T.P. Hanusa, Organometallics 19 (2000) 1556;
(e) K. Fichtel, K. Hofmann, U. Behrens, Organometallics 23 (2004) 4166;
(f) T. Hatanpää, M. Ritala, M. Leskelä, J. Organomet. Chem. 692 (2007) 5256;
(g) G.B. Deacon, C.M. Forsyth, F. Jaroschik, P.C. Junk, D.L. Kay, T. Maschmeyer, A.F. Masters, J. Wang, L.D. Field, Organometallics 27 (2008) 4772;
(h) D.P. Daniels, G.B. Deacon, D. Harakat, F. Jaroschik, P.C. Junk, Dalton Trans. 41 (2012) 267.
[4] S.A. Kinsley, A. Streitwieser, A. Zalkin, Organometallics 4 (1985) 52;
(b) D.S. Hutchings, P.C. Junk, W.C. Patalinghug, C.L. Raston, A.H. White, J. Chem. Soc., Chem. Commun. (1989) 973;
(c) M.D. Walter, G. Wolmershäuser, H. Stizmann, J. Am. Chem. Soc. 127 (2005) 17494.
[5] E. Beckman, K. Beck, H. Schlegel, Chem. Dtsch. Ber. Ges. 38 (1905) 904.
[6] (a) G. Moesges, F. Hampel, P.V. R Schleyer, Organometallics 11 (1992) 1769;
(b) K. Fichtel, S. Höxter, U. Behrens, Z. Anorg, Allg. Chem. 632 (2006) 2003.
[7] F. Feil, S. Harder, Eur. J. Inorg. Chem. 2003 (2003) 3401.
[8] J.S. Overby, T.P. Hanusa, Organometallics 15 (1996) 2205.
[9] H. Li, B. Wei, L. Xu, W.-X. Zhang, Z. Xi, Angew Chem. Int. Ed. Engl. 52 (2013) 10822.
[10] J.S. Alexander, K. Ruhlandt-Senge, Eur. J. Inorg. Chem. 11 (2002) 2761.
[11] B. Bogdanović, Acc. Chem. Res. 21 (1988) 261.
[12] (a) A. Weeber, S. Harder, H.H. Brintzinger, Organometallics 19 (2000) 1325;
(b) F. Feil, S. Harder, Organometallics 20 (2001) 4616.
[13] J.B. Claridge, Y. Kubozono, M.J. Rosseinsky, Chem. Mater. 15 (2003) 1830.
[14] M.S. Hill, D.J. Liptrot, C. Weetman, Chem. Soc. Rev. 45 (2016) 972.
[15] (a) A.S. Filatov, A.V. Zabula, S.N. Spisak, A.Yu Rogachev, M.A. Petrukhina, Angew. Chem. Int. Ed. 53 (2014) 140;
(b) S.N. Spisak, A.Yu Rogachev, A.V. Zabula, A.S. Filatov, R. Clérac, M.A. Petrukhina, Chem. Sci. 8 (2017) 3137;
(c) Z. Zhou, S.N. Spisak, Q. Xu, A.Yu Rogachev, Z. Wei, M. Marcaccio, M.A. Petrukhina, Chem. Eur J. 24 (2018) 3455;
(d) A.V. Zabula, S.N. Spisak, A.S. Filatov, A.Yu Rogachev, M.A. Petrukhina, Acc. Chem. Res. 52 (2018) 1541.
[16] K. Mochida, T. Yamanishi, J. Organomet. Chem. 332 (1987) 247.
[17] (a) M.J. Mccormick, K.B. Moon, S.R. Jones, T.P. Hanusa, J. Chem. Soc., Chem. Commun. (1990) 778;
(b) H. Bönnemann, B. Bogdanović, R. Brinkmann, B. Spliethoff, J. Organomet. Chem. 451 (1993) 23.
[18] S.R. Drake, D.J. Otway, J. Chem. Soc., Chem. Commun. (1991) 517.
[19] (a) V. Grignard, Comptes Rendus 198 (1934) 625;
(b) D.E. Pearson, D. Cowan, J.D. Beckler, J. Org. Chem. 24 (1959) 504.
[20] D.Y. Chang, N. Shieh, J. Chin. Chem. Soc. 1 (1954) 64.
[21] W.L. Respess, J.P. Ward, C. Tamborski, J. Organomet. Chem. 19 (1969) 191.
[22] (a) B.R. Aluri, Synlett 10, 2008, p. 1579;
(b) A. Lorbach, C. Reus, M. Bolte, H. Lerner, M. Wagner, Adv. Synth. Catal. 352 (2010) 3443.
[23] N.J. O'Neil, Ph.D. Dissertation, University at Albany, Albany, NY, 2017.
[24] T. Wu, H. Xiong, R.D. Rieke, J. Org. Chem. 55 (1990) 5045.
[25] A.G. Goos, P.J.R. Flores, Y. Takahashi, K. Ruhlandt-Senge, Alkaline earth metals: organometallic chemistry, in: R.A. Scott (Ed.), Encyclopedia of Inorganic Chemistry, second ed., Wiley, New Jersey, 2012, pp. 1–38.
[26] D.M. Roitershtein, L.F. Rybakova, E.S. Petrov, A.M. Ellern, M.Y. Antipin, Y.T. Struchkov, J. Organomet. Chem. 460 (1993) 39.
[27] (a) C.T. Brock, J.D. Dunitz, Acta Crystallogr. B46 (1990) 795;

(b) A. Matsumoto, M. Suzuki, H. Hayashi, D. Kuzuhara, J. Yuasa, T. Kawai, N. Aratani, H. Yamada, Bull. Chem. Soc. Jpn. 90 (2017) 667.
[28] (a) W.E. Rhine, J. Davis, G. Stucky, J. Am. Chem. Soc. 97 (1975) 2079;
(b) L.M. Engelhardt, S. Garvey, C.L. Raston, A.H. White, J. Organomet. Chem. 341 (1988) 39;
(c) H. Bock, K. Gharagozloo-Hubmann, M. Sievert, T. Prisner, Z. Havlas, Nature 404 (2000) 267;
(d) C. Jones, L. Mcdyre, D.M. Murphy, A. Stasch, Chem. Commun. 46 (2010) 1511.
[29] M.D. Fryzuk, L. Jafarpour, F. M Kerton, J.B. Love, S.J. Rettig, Angew. Chem. Int. Ed. 39 (2000) 767.
[30] S.G. Boué, C.G. Jung, J. Castillo, E.V. Donckt, J. Chem. Soc., Perkin Trans. 2 (1996) 1691.
[31] L. Li, H. Wang, W. Wang, W.J. Jin, CrystEngComm 19 (2017) 5058.
[32] H. Bock, C. Arad, C. Näther, J. Organomet. Chem. 520 (1996) 1.
[33] J. Smid, J. Am. Chem. Soc. 87 (1965) 655.
[34] I. Fedushkin, M.N. Bochkarev, H. Schumann, L. Esser, G. Kociok-Köhn, J. Organomet. Chem. 489 (1995) 145.
[35] D.D. Ebbing, Ionic and covalent bonding, in: M.S. Wrighton (Ed.), General Chemistry, fifth ed., Houghton Mifflin, Boston, 1996, pp. 343–386.
[36] C. P Brock, J.D. Dunitz, Acta Crystallogr. Sect. B Struct. Crystallogr. Cryst. Chem. 38 (1982) 2218.
[37] (a) J.J. Brooks, W. Rhine, G.D. Stucky, J. Am. Chem. Soc. 94 (1972) 7346;
(b) C. Melero, A. Guijarro, M. Yus, Dalton Trans. (2009) 1286.
[38] (a) A.V. Protchenko, L.N. Zakharov, M.N. Bochkarev, J. Organomet. Chem. 447 (1993) 209;
(b) M.N. Bochkarev, I.L. Fedushkin, A.A. Fagin, H. Schumann, J. Demtschuk, Chem. Commun. (1997) 1783;
(c) W. Huang, S.I. Khan, P.L. Diaconescu, J. Am. Chem. Soc. 133 (2011) 10410;
(d) W. Huang, P.L. Diaconescu, Eur. J. Inorg. Chem. 2013 (2013) 4090;
(e) A.N. Selikhov, T.V. Mahrova, A.V. Cherkasov, G.K. Fukin, E. Kirillov, C.A. Lamsfus, L. Maron, A.A. Trifonov, Organometallics 35 (2016) 2401.
[39] N.V. Kozhemyakina, J. Nuss, M. Jansen, Z. Anorg, Allg. Chem. 635 (2009) 1355.
[40] G.R. Fulmer, A.J.M. Miller, N.H. Sherden, H.E. Gottlieb, A. Nudelman, B.M. Stoltz, G.R.J.E. Bercaw, K.I. Goldberg, Organometallics 29 (2010) 2176.
[41] SAINT, Part of Bruker APEX3 Software Package (Version 2016), Bruker AXS, 2016.
[42] SADABS, Part of Bruker APEX3 Software Package (Version 2016), Bruker AXS, 2016.
[43] G.M. Sheldrick, SHELXT; version 2018/2, Acta Crystallogr. A71 (2015) 3.
[44] G.M. Sheldrick, XL refinement program version 2018/3, Acta Crystallogr. C71 (2015) 3.
[45] A.L. Spek, SQUEEZE; subroutine of PLATON (version 230318), Acta Crystallogr. C71 (2015) 9.